Taylor & Francis
Taylor & Francis Group

Time-dependent analysis of heat transfer enhancement and entropy generation of hybrid nanofluids in a tube with a solid and elliptical–cut twisted tape insert with non-uniform heat flux

Amir Mohamad Khfagi, Graeme Hunt, Manosh C Paul & Nader Karimi

Published online: 18 Sep 2023.

Submit your article to this journal ☐

Article views: 21

View related articles ☐

View Crossmark data ☐

Taylor & Francis
Taylor & Francis Group

🔓 OPEN ACCESS | Check for updates

Time-dependent analysis of heat transfer enhancement and entropy generation of hybrid nanofluids in a tube with a solid and elliptical-cut twisted tape insert with non-uniform heat flux

Amir Mohamad Khfagi[a], Graeme Hunt[a], Manosh C Paul[a], and Nader Karimi [ID][a,b]

[a]James Watt School of Engineering, University of Glasgow, Glasgow, UK; [b]School of Engineering and Materials Science, Queen Mary University of London, London, UK

ABSTRACT

This numerical study investigates the improvement of transient heat transfer in a plain tube using hybrid nanofluids consisting of solid particles and twisted tapes with elliptical cuts, under non-uniform heat flux conditions. The analysis includes the calculation of the Bejan number and entropy production. Different working fluids, including water, CuO/water nanofluid, and a hybrid nanofluid with a 2% volume concentration of Al_2O_3-Cu/water, are used with varying concentrations of the hybrid nanofluid ranging from 1% to 4%. Effects of heat flux distribution and local concentration ratio (LCR) are investigated. The computational results indicate that conventional and elliptical cut twisted tapes enhance transient heat transmission. A slight rise in the heat transfer coefficient is observed when the fluid has higher thermal conductivity. The flow velocity gradually stabilizes over time. The hybrid nanofluid of (Al_2O_3-Cu/water) significantly affects transient heat transmission, reducing the maximum temperature difference by approximately 4.1% compared to water and 6.2% compared to the nanofluid. Transient heat transmission is further intensified by TECT. Moreover, frictional entropy production dominates the system's irreversibility. This study contributes to the understanding of transient heat transfer enhancement and its dependence on hybrid nanofluids, providing insights for engineering applications.

Introduction

Solar receiver tubes have a crucial function in converting solar radiation into thermal energy within parabolic trough systems, comprising approximately 30% of the material expenses involved in constructing a solar field (Wu et al. 2014). Solar thermal energy is effective in many applications, including solar heating of water, solar chemistry (Krüger et al. 2008), solar desalination plants, and concentrating solar power plants (Hepbasli and Alsuhaibani 2011). Recently, solar-thermal engineering has focused on optimizing parabolic trough concentrators for industrial applications. In parabolic trough tubes, excessive absorber tube circumferential temperature variations produce thermal strains and may damage the receiver's glass cover (Muñoz and Abánades 2011). Several investigations on receiver thermal performance have demonstrated that greater absorber pipe temperatures lead to increased receiver thermal losses (Burkholder and Kutscher 2008). It is also expected that high optical efficiency and concentration ratios would result in large heat fluxes and circumferential temperature differences in absorber tubes (Mwesigye, Bello-Ochende, and Meyer 2016). As a result, better performance of heat transmission is required to reduce absorber tube temperature gradients and increase receiver performance and reliability.

Previous research has focused on enhancing heat transmission in pipes using twisted-tape inserts under uniform heat flow with steady flow conditions (Ahmadi et al. 2020; Oni and Paul 2016). Sharma et al. examined pressure drop and heat transport in a duct with twisted tape inserts utilizing Al_2O_3/water in the transitional flow range (Sharma, Sundar, and Sarma 2009). Esmaeilzadeh et al. studied the friction factor and heat transmission characteristics of Al_2O_3/water in plain pipes with twisted tape inserts of varying thicknesses (Esmaeilzadeh et al. 2014). Another approach to enhancing heat transfer in pipes involves the use of liquid-solid particle mixtures. A study conducted by Khfagi et al. (2022) revealed a significant increase in heat transfer when altering fluid thermal conductivity and dynamic viscosity. Nakhchi and Esfahani (2018) conducted an empirical investigation exploring the utilization of various nanofluids as working fluids within pipes equipped with conventional twisted tape. Their findings revealed that the incorporation of nanofluids resulted in enhanced thermophysical characteristics, elevated heat transmission coefficients, and improved thermal efficiency when compared to the use of pure water. In a study of nanofluid flow in circular ducts, twisted tape inserts were examined by Sundar and Sharma (2010), who observed a noteworthy 33.51% enhancement in the heat transfer coefficient with Al_2O_3-water nanofluids. Additionally, Jafaryar, Sheikholeslami, and Li (2018) conducted numerical investigations on CuO-water nanofluid flow in a heat exchanger using twisted tape, finding that an increase in the number of tape revolutions resulted in an increase in secondary flow.

Many studies have used analytical approaches, experiments, and numerical simulations to estimate heat transmission for non-uniform heat flux in ordinary tubes. However, relatively few studies have explored convective heat transmission in pipes with twisted tape and non-uniform heat flux. Using non-uniform heating conditions, Kinoshita et al. (1996) developed a method for amplification of the critical flow temperature for boiling fluid using internal twisted tape, which was carried out in a twisted tape tube. The geometric impact of twisted tape, on the other hand, has not been examined. Chang, Li, and Zhang (2014) and Yang et al. (2012) explored the turbulent heat transport convection of a non-uniform heat flow through a solar receiver pipe using computational fluid dynamics (CFD) experimentally and computationally, respectively. The effect of twisted tapes on heat transport within a molten salt solar absorber pipe experiencing unidirectional heat flow was examined by Chang et al. (2015). Afsharpanah et al. (2021) examined the effects of twisted tape on pressure drop, heat transmission, and then thermal efficiency within solar trough collectors, utilizing various twisted tape designs such as perforated, square cut, v-cut, and center-cleared inserts. Considering the non-uniform heat flow nature of collectors in parabolic troughs, their findings revealed that twisted tape exhibits superior thermal efficiency compared to plain tubes.

Analyzing the transient thermal behavior of parabolic trough solar collector tubes is crucial for optimizing the utilization of solar thermal energy in response to varying solar radiation conditions. Transients in heat transfer and diffuse solar irradiation have been identified and explained by the authors (Li et al. 2017, 2019). The performance of the collectors of parabolic troughs in transient processes was investigated by Xu et al. (2013). A 3D thermal-hydraulic simulation of a reactor of high-temperature engineering test was calculated by Tochio and Nakagawa (2011). They computed steady-state and unsteady-state values. Researchers at Kobe University (Liu, Zhao, and Fukuda 2014) found experimental results and correlations for simultaneous helium gas flow through a plate and a horizontal cylinder with an exponentially rising rate of heat production. Under a variety of experimental conditions, the diameter and geometry of heaters were evaluated for their effects on transient heat transmission. However, the majority of studies investigated such heat transfer increases employing twisted tape exclusively under steady flow conditions: a uniform temperature or heat flow wall. Transient heat transmission for tubes with twisted tapes has been documented rarely. Similarly, researchers at Kobe University (Liu, Zhao, and Fukuda 2015) extended their studies to a wide range of transient heat transmission augmentations for helium gas based on twisted tapes. They found that the pitch of the twisted tape had a substantial effect on the coefficient of heat transmission. The Nusselt number was found to be almost 50% greater than the flat plate.

The majority of studies examining the performance analysis of tubes, with or without twisted tape, focus primarily on the application of the first law of thermodynamics, which does not

provide insights into the energy quality generated by parabolic trough systems. To gain a better understanding of the energy quality within these systems and optimize their thermal efficiency, the second law of thermodynamics is frequently utilized (Bejan 2013). Numerous studies on entropy generation have been conducted using heat transmission augmentation methods. Heat transport and generation of entropy in one of the parabolic troughs with wall-mounted twisted tape insertions are illustrated in Jaramillo et al. 2016; Mwesigye, Bello-Ochende, and Meyer (2016). Sheikholeslami, Jafaryar, and Li (2018) considered the entropy creation in a channel with nano-fluid flow induced by twisted tape. For the entropy generation study on non-uniform heat flux, recent research by Mwesigye, Bello-Ochende, and Meyer (2014) examined the formation of minimum entropy creation in a receiver of the parabolic trough with non-uniform flow of heat at varying rim angles and ratios of concentration owing to fluid friction and transmission of heat. The results reveal that for any combination of heat, ratio of concentration, and rim angle, the creation of total entropy is reduced. The generation of total entropy raised with decreasing rim angle, ratio of concentration, and fluid temperature.

The literature review emphasizes several crucial aspects regarding heat transmission and entropy production in parabolic receivers. Firstly, the potential enhancement of transient heat transfer through the utilization of twisted tape in parabolic trough collector tubes remains insufficiently examined. Secondly, there is a current dearth of research exploring transient heat transfer rates in parabolic trough receivers under non-uniform heat flux conditions, both in the presence and absence of twisted tape inserts. Thirdly, with the exception of Mwesigye, Bello-Ochende, and Meyer (2014) who examined the formation of minimum entropy in a receiver with non-uniform heat flow, there is a lack of research on entropy production due to transient heat transfer in pipes, both with and without twisted tape, as well as non-uniform heat flux. Furthermore, the specific characteristics of tube transient heat transfer rates have received inadequate attention.

It is worth noting that transient heat transmission is of paramount importance in diverse engineering applications, significantly impacting system efficiency and performance. However, investigations into entropy creation and transient heat transmission in turbulent flows within parabolic troughs (PT), twisted pipe (TPT), and twisted elliptical cross-section tubes (TECT) using hybrid nanofluids have been relatively overlooked. Previous work has primarily focused on entropy creation analysis and thermohydraulics in TECT, TPT, and PT under steady flow and uniform heat flow conditions (Khfagi et al. 2022). To bridge this research gap, the present study conducts computational analyses to explore the transient heat transfer rate and analyze entropy creation in turbulent flow scenarios involving Al_2O_3-Cu/water, CuO/water, and water for PT, TPT, and TECT subjected to circumferentially non-uniform heat flux.

Numerical approaches

Physical model and boundary conditions of TECT, TPT, and PT

The study of the physical models was created and implemented in the program Star CCM+: Three Dimensional, The Reynolds Averaged Navier-Stokes, Implicit Unsteady (suitable for water, nanofluid, and hybrid-nanofluid) and Segregated Flow Temperature. The turbulent flow simulation is implemented via the realizable k-ε turbulence model. For the parameters of near wall, the STAR-CCM+ two-layer model with all y+ wall function is used. This technique has the potential to provide an accurate assessment of near wall viscous flow. To achieve a better level of temporal precision, a transient simulation with a time step of $\Delta t = 0.001$ seconds is conducted. This investigation was conducted under the following boundary conditions:

(1) The geometry used in this investigation is shown in Figure 1 and Table 1.

(2) The outer wall of the pipe experiences non-uniform heat flow, with a receiver angle (θ) of 40°. The distribution of heat flux and local concentration ratios utilized in this investigation are depicted in Figures 4 and 5 and determined by Equations 1 and 22.
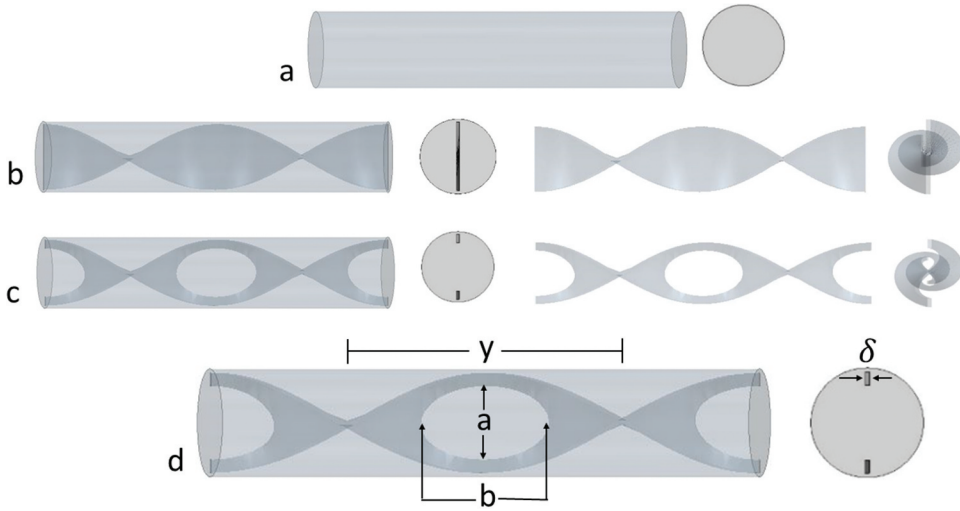
Figure 1. Models (a) (PT), (b) (TPT), (c) (TECT), and (d) schematic of twisted tape.

Table 1. Geometric characteristics of the investigated tubes.

Feature	Value	Feature	Value
D	0.0195	y	0.057 m
L	1 m	a/w	0.7
w	0.019 m	b/a	2
δ	0.0008 m		

$$q = h(T_{ri} - T_{bulk}) \tag{1}$$

For turbulent flows, the heat transfer coefficient in STAR-CCM+ as in Equation 2.

$$h = \frac{\rho_{fp.f} u}{T} \tag{2}$$

$$q = \frac{\rho_{fp.f} u}{T}(T_{ri} - T_{bulk}) \tag{3}$$

(3) Both the duct wall and the surface of solid and elliptical twisted tape are non-slip surfaces.

(4) Fluid enters the pipe at 25Cº (Li et al. 2019), and Reynolds number is 20,000.

(5) Water, nanofluid of CuO/water, and hybrid nanofluid of Al_2O_3-Cu/water are used as the working fluids. Nanoparticle concentration is $\emptyset = 2\%$.

(6) Al_2O_3-Cu/water hybrid-nanofluids with varying volume concentrations ranging from 1% to 4% were utilized as the working fluids for TECT.

(7) The thermophysical characteristics of hybrid-nanofluid have been determined by our previous work (Khfagi et al. 2022).

Governing equation

The following transport equations describe the behavior of continuum (both solid and fluid) (Langtry 2006): Continuity equation, Momentum equation, and Energy equation, respectively.

$$\frac{\partial}{\partial t}(\rho) + \frac{\partial}{\partial x_i}(\rho u_i) = 0 \tag{4}$$

$$\frac{\partial}{\partial t}(\rho u_i) + \frac{\partial}{\partial x_j}(\rho u_i u_j) = -\frac{\partial p}{\partial x_i} + \frac{\partial}{\partial x_j}\left\{\mu_{eff}\left(\frac{\partial u_i}{\partial x_j} + \frac{\partial u_j}{\partial x_i}\right) - \frac{2}{3}\mu_{eff}\frac{\partial u_l}{\partial x_l}\delta_{ij}\right\} \tag{5}$$

In this equation, p is the static pressure, u is velocity, , ρ is dynamic viscosity, and the effective viscosity is calculated as the product of laminar and turbulent viscosities:

$$\mu_{eff} = \mu + \mu_t \tag{6}$$

The conservation of energy balance is expressed as (Dixon, Nijemeisland, and Stitt 2006),

$$\frac{\partial}{\partial t}(\rho u_i) + \frac{\partial}{\partial x_j}(\rho u_j C_p T) = \frac{\partial}{\partial x_j}\left(k_{eff}\frac{\partial T}{\partial x_j} + \frac{\mu_t}{\sigma_{h.t}}\frac{\partial(C_p T)}{\partial x_j}\right) + u_j\frac{\partial p}{\partial x_i}$$
$$+ \left[\mu_{eff}\left(\frac{\partial u_i}{\partial x_j} + \frac{\partial u_j}{\partial x_i}\right) - \frac{2}{3}\mu_{eff}\frac{\partial u_i}{\partial x_i}\delta_{ij}\right]\frac{\partial u_i}{\partial x_j} \tag{7}$$

The realizable k-ε model, introduced by (Shih 1993), represents a significant advancement in turbulence modeling. This particular model demonstrates enhanced predictive capabilities, especially when it comes to estimating flow velocities in intricate flow configurations like those involving twisted tape inserts.

Equation of kinetic energy (k) of turbulence:

$$\frac{\partial(\rho k)}{\partial t} + \frac{\partial(\rho k u_i)}{\partial x_i} = \frac{\partial}{\partial x_j}\left[\left(\mu + \frac{\mu_t}{\sigma_k}\right)\frac{\partial k}{\partial x_j}\right] + G_k - \rho\varepsilon \tag{8}$$

Equation of turbulence dissipation rate (ε)

$$\frac{\partial(\rho\varepsilon)}{\partial t} + \frac{\partial(\rho\varepsilon u_i)}{\partial x_i} = \frac{\partial}{\partial x_j}\left[\left(\mu + \frac{\mu_t}{\sigma_\varepsilon}\right)\frac{\partial\varepsilon}{\partial x_j}\right] + \rho C_1 S_\varepsilon - \rho C_2\frac{\varepsilon^2}{k + \sqrt{(\mu/\rho)\varepsilon}} \tag{9}$$

The viscosity of turbulent, μ_t, is determined based on the turbulent kinetic energy (k) and the dissipation rate (ε). $\mu_t = \rho C_\mu \frac{k^2}{\varepsilon}$
where G_k is the creation of the kinetic energy of turbulent and was produced similarly to all k-ε models as:

$$G_K = \frac{\partial u_j}{\partial x_i}\mu_t\left(\frac{\partial u_i}{\partial x_j} + \frac{\partial u_j}{\partial x_i}\right) - \frac{2}{3}\left(\rho k + \mu_t\frac{\partial u_i}{\partial x_i}\right)\delta_{ij} \tag{10}$$

Model coefficients C_1 and $_\mu$ for the realizable k-ε model is determined by the following equations (Versteeg and Malalasekera 2007)

$$C_1 = max\left[0.43, \frac{\eta}{\xi + 5}\right], \xi = S\frac{k}{\varepsilon}, S \equiv \sqrt{2S_{ij}S_{ij}}$$

The other empirical constants are described by (Versteeg and Malalasekera 2007): $\sigma_\varepsilon = 1.2\, C_2 = 1.9$. S_{ij} represents the rate at which a fluid in motion linearly deforms (Versteeg and Malalasekera 2007):

$$S_{ij} = \frac{1}{2}\left(\frac{\partial u_i}{\partial x_i} + \frac{\partial u_i}{\partial x_j}\right) \tag{11}$$

Entropy creation

In each scenario, the rate of local entropy creation was calculated, with only thermal and frictional impacts considered:

$$S_{g,t} = S_{HT} + S_{FF} \qquad (12)$$

Generally, the creation of volumetric entropy within a system is commonly expressed in the following manner (Mwesigye, Bello-Ochende, and Meyer 2013):

$$S_{HT} = \frac{k_c}{T^2} \left(\frac{\partial T}{\partial x_i} \right)^2 \qquad (13)$$

$$S_{FF} = \frac{\mu}{T} \left\{ 2 \left[\left(\frac{\partial u_i}{\partial x_i} \right)^2 \right] + \left(\frac{\partial u_i}{\partial x_j} + \frac{\partial u_j}{\partial x_i} \right)^2 \right\} \qquad (14)$$

By incorporating the individual components of volumetric entropy creation across the duct volume, the total entropy production ($S_{g,t}$) is calculated.

$$S_{g,t} = \left\{ {}^{S_{HT}} + {}^{S_{FF}} \right\} \partial V \qquad (15)$$

The Be is commonly utilized to quantify the contribution of each irreversibility to the overall rate of total entropy creation. Its definition is provided by (Sheikholeslami, Jafaryar, and Li 2018)

$$Be = \frac{S_{HT}}{S_{g,t}} \qquad (16)$$

Numerical analysis

The commercial software program Star-CCM+ was employed for the numerical solution, encompassing geometry design and computational grid generation. The software utilizes a finite volume approach to solve the governing equations, including continuity, momentum, energy, and the k-ε model, as outlined in Section 2.1. The velocity-pressure coupling is performed using Patankar and Spalding's Semi-Implicit Pressure Linked Equations (SIMPLE) approach (Patankar and Spalding 1983). To obtain a converged temperature solution for unsteady flow, a second-order accurate time integration scheme is employed. Turbulent flow conditions are considered for analyzing the temperature distribution in PT, TPT, and TECT. The obtained results are compared with experimental and numerical data from previous studies (Boz, Erdogdu, and Tutar 2014; Heng et al. 2019; Li et al. 2019). Furthermore, MATLAB was used for solving Equation 13–16.

Results and discussion

Grid independence test

An investigation of the grid independence of numerical computations was performed for temperature as a monitored quantity by using four sizes of various mesh for PT, TPT, and TECT before settling on a mesh size of 842,500, 2,779,954, and 4,661,961 cells, respectively. In order to capture the flow features around the twisted tape, we refined the mesh in the regions on and near the twisted tape. This typically involves creating a denser grid with smaller element sizes near the twisted tape and its immediate vicinity. To apply enhanced wall function technique, the wall y+ is strictly controlled between 35 and 100 (Abuhatira, Salim, and Vorstius 2021). Figure 2 demonstrates the temperature test results for the grid resolution. The
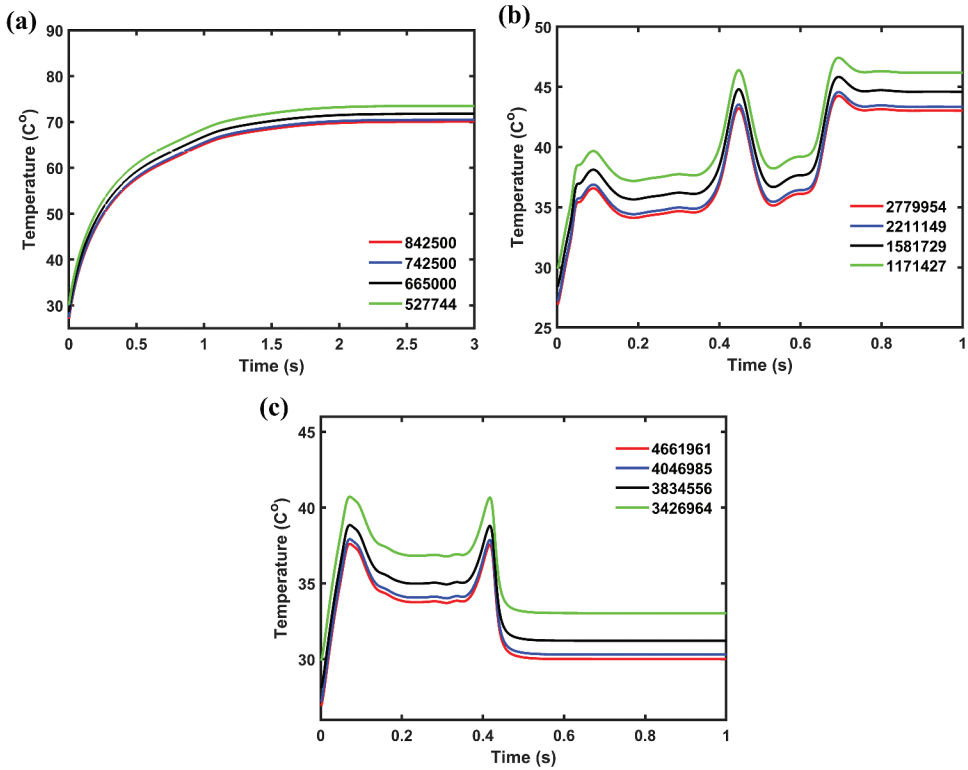
Figure 2. Temperature at a selected point in the middle (a) PT, (b) TPT, and (c) TECT.

values of temperature obtained in grids with total cell counts of 665,000, 742500, and 842,500 differ by 2.4%, 3.9%, and 4.6% from those found in a grid with 527,744 cells, respectively, in the PT (frame (a)). The TPT (frame (b)) indicates a difference of 3.4%, 6.2%, and 6.8% when comparing the temperature readings of grids containing 1,581,729, 2211149, and 2779954 cells to those of grid containing 1,171,427 cells. In TECT (frame (c)), there is an alteration of 5.5% %, 8.2%, and 9% when comparing the temperature readings in grids with 3,834,556, 4046985, and 4,661,961 cells to those in grid with 3,426,964 cells.

Courant number analysis in Eq. 21 is necessary because the solutions' stability is critical to accuracy. According to Anderson and Wendt (1995), the Courant number should be less than or equal to 1. This is a significant stability criterion for maintaining equilibrium. It limits how long a time step may be or mesh cell size, and finer meshes require smaller time steps.

$$Co = u.\frac{\Delta t}{\Delta x} \leq 1 \qquad (17)$$

Here Co is courant number, u is velocity, Δx is the grid cell dimension at each point, and Δt is time-step. Also, an independence of time step investigation regarding unsteady calculation was conducted. Different values of the time steps, (Δt) from 0.01 s to 0.09 s were selected, resulting in slight variations. The size of time step has been investigated from 0.0005 to 0.0015. When $\Delta t < 0.001$, the influence of the time step size is insignificant.

Model validation

Numerical computations of the present study are validated by Ahmet Tandiroglu's research (Tandiroglu 2005), which investigated a turbulent flow with (Re = 10366). Figure 3 shows that a circular duct with baffle
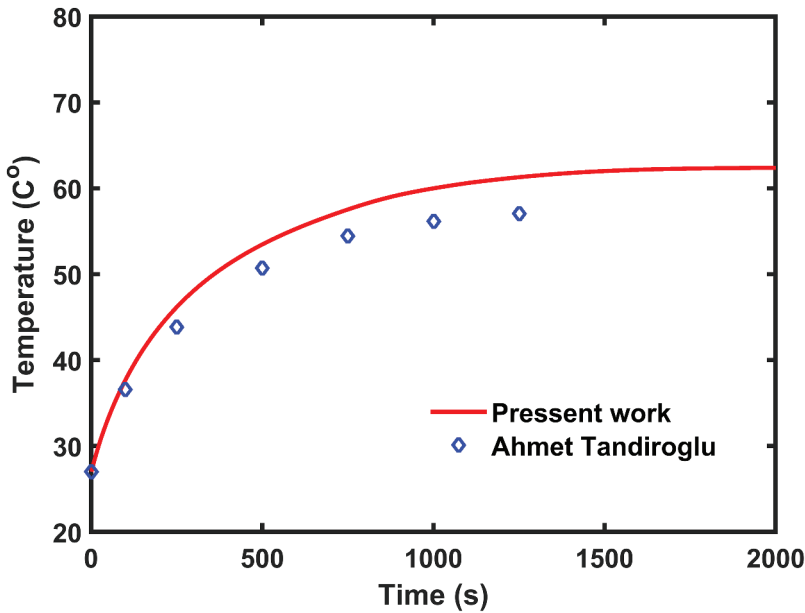
Figure 3. The variation of temperature against time Ahmet Tandiroglu (Tandiroglu 2005).
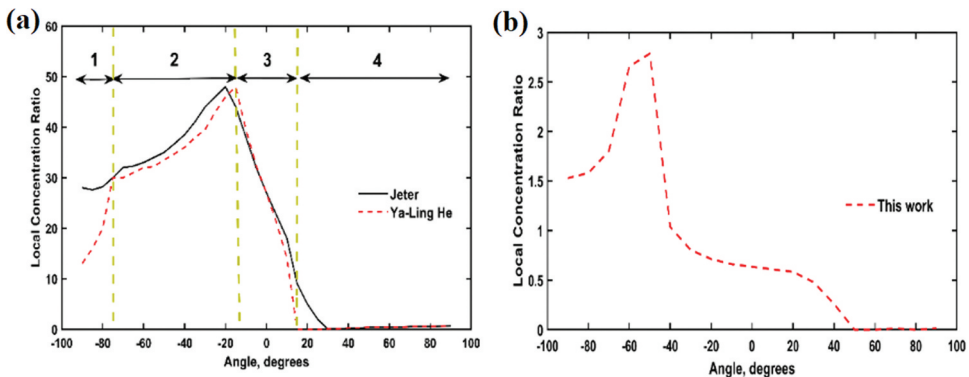

Figure 4. Local concentration ratios distribution.

plate inserts (Tandiroglu 2005) was employed to validate a circular tube (PT) for transient forced convective heat transmission. The investigation was conducted using air with a Prandtl number of 0.71. In Figure 3, the outlet temperature change curves from this study and the work by Ahmet Tandiroglu are compared. Based on the observed data, it is evident that their similarities are considerable. The temperature variation curve of the present work deviates from those of Ahmet Tandiroglu by ±6.9%, which is considered acceptable.

Distribution of local concentration ratio (LCR)

Optimizing the parabolic trough solar collector shape involves analyzing the LCR rate on the receiver pipe using Monte Carlo Ray-Trace (MCRT). To validate this approach, numerical results were compared to studies by He et al. (2011), Jeter (1987), and Marugán-Cruz et al. (2016). Jeter (1987) focused on the LCR parameter, similar in nature to the distribution of heat flow. The correlation between the two parameters is illustrated in (He et al. 2011; Jeter 1987):
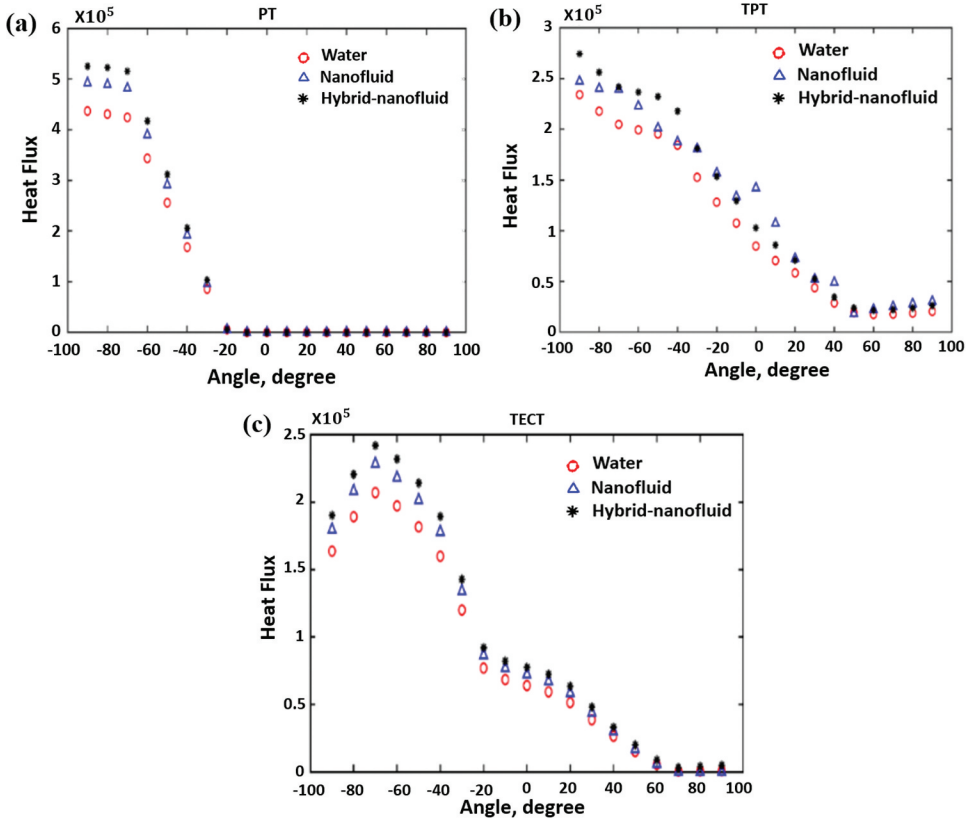
Figure 5. Heat flux distribution on circle direction for three different tubes.

$$q = LCR.q_{sun} \qquad (18)$$

The curve in Figure 4 can be split into four parts, denoted by 1, 2, 3, and 4 as discussed by (He et al. 2011). Note that the MCRT resolves under different conditions. While the findings presented in this paper may not align completely with the outcomes reported in He et al. (2011) and Jeter (1987), the overall trends exhibited by the curves are remarkably similar. Figure 4(b) illustrates that the computed outcomes of LCR are in agreement with the results of He et al. (2011) and Jeter (1987) when solar rays are considered to be parallel rays. As well, the LCRs in Ref (Marugán-Cruz et al. 2016) show the same trend. According to the results, MCRT's probability model in this paper is reasonable.

Distribution of heat flow

The heat flow distribution on the outer surface of the pipe is displayed in Figure 5(a) for PT, (b) for TPT, and (c) for TECT. Due to the symmetry, only one half of the receiver, i.e., $-90° \leq \theta \leq 90°$, may be considered. As observed in Figure 5, the profile of heat flux around the absorber tube's circumference varies greatly because of the used elliptical-cut and classical twisted tape inserts. In addition, when twisted tape is inserted, the heat flux increases as the collector rim angle increases. The finite temperature difference will be increased because of the increase in peak heat flux. Furthermore, at $\theta > 30°$, the heat flux profile consists of a direct radiation area (as seen in part 4 in Figure 4(a)). In the case of different fluid flows, hybrid-nonfluids are shown to give high heat flux peaks and will give high absorber tube
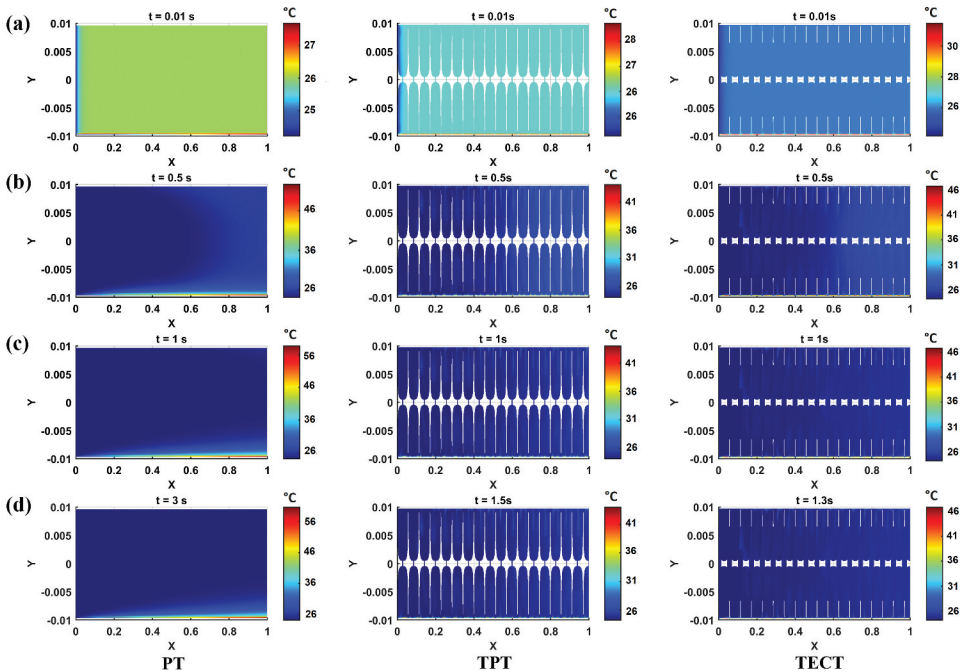
Figure 6. Temperature distribution of Al$_2$O$_3$-Cu/water hybrid nanofluid flow within PT, TPT, and TECT at various times.

circumferential temperature gradients. The calculated results in this paper closely match the receiver results for half the circumference (Mwesigye, Bello-Ochende, and Meyer 2014).

Temperature contour

Four distinct temporal situations were studied to examine the influence of temperature on Al$_2$O$_3$-Cu /water in Figure 6. PT is (0.01 s, 0.05 s, 1 s, and 3 s), TPT is (0.01 s, 0.05 s, 1 s, and 1.5 s), and TECT is (0.01 s, 0.05 s, 1 s, and 1.3 s). Figure 6 (frames A-C) illustrates the simulation's temporal evolution from 0.01 s to 1 s. Figure 6 (frame D) shows the time when the simulation solved the problem. In PT Figure 6, the simulation findings reveal that the temperature distribution in the pipe is significantly non-uniform due to non-uniform heat flow on the outer pipe wall. At exit, TPT and TECT have a more uniform temperature distribution than PT. One potential reason is that while the liquid is progressively heated along the direction of flow, the elliptical-cut and plate twisted tape help increase the distributions of temperature along the tube length in the flow direction. The tube will thus be able to distribute temperature more evenly. In addition, the findings show that the thermal layer near the wall of the duct grows faster in the TPT and TECT than in the PT and grows even more over time. From Figure 6 (frame D), the temperature for Al$_2$O$_3$-Cu/Water in the PT, TPT, and TECT are 56C^o, 41C^o, and 46C^o, respectively. One of the most notable benefits of TPT and TECT, as shown in Figure 6, is that the distribution of temperature is considerably more uniform on all surfaces of the tube. From 0.01 s to the end of the simulation, the temperature differences of up to 29C^o, 13C^o, and 16C^o occur between PT, TPT, and TECT. This temperature data is very useful for designing, optimizing, controlling, and maintaining parabolic trough collectors.

Turbulent kinetic energy contour

Figure 7 explains the time histories of turbulent kinetic energy for three unsteady flow conditions (PT, TPT, and TECT) using a hybrid-nanofluid of Al$_2$O$_3$-Cu/water. Obviously, for Figure 7 (frame A), the
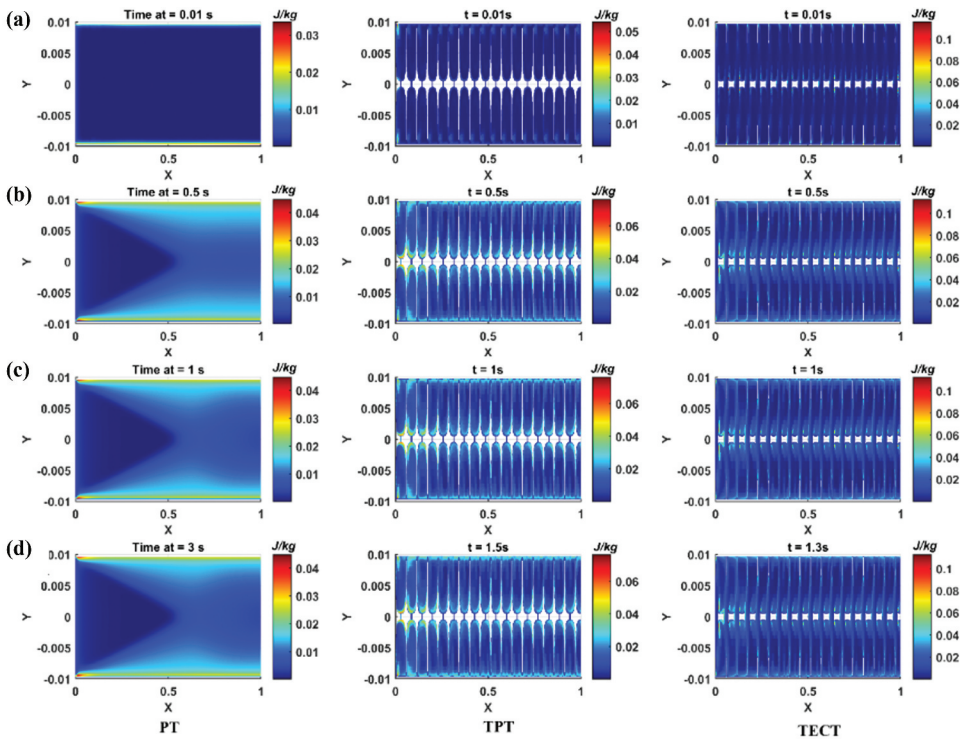
Figure 7. Turbulent kinetic energy distribution of Al_2O_3-Cu/water hybrid flow within PT, TPT, and TECT at various times.

prediction for the turbulent kinetic energy in the wall region is almost indistinguishable during the early time of the three flows. However, as the time progresses in unsteady flow simulations, the changes in turbulent kinetic energy become more pronounced. This is because larger time allows for larger fluctuations in fluid motion, which can lead to the production of more turbulent kinetic energy. As seen in PT Figure 7 (frame B-D), the highest amount of the turbulent kinetic energy was located close to the wall, because of the low flow velocity caused by the no-slip condition on the wall (Oni and Paul 2016). As compared to the PT, the TECT and TPT have more turbulent kinetic energy. This is because the tape makes the boundary layer more turbulent (Oni and Paul 2016). The findings indicate that TECT significantly increases the intensity of flow between the core area and the pipe wall. Comparatively to conventional twisted tapes, this type of modified tape may significantly increase flow interruptions and mixing of hot and cold flows. In accordance with this finding, our prior study (Amir Mohamad Khfagi et al. 2023) and that of (Ahmadi et al. 2020) are consistent with this finding.

Transient heat transfer for PT, TPT, and TECT

Figure 8 depicts three temperature variation curves obtained from STAR-CCM+ simulations of Al_2O_3 -Cu/water, CuO/water, and water during periods with time 3, 1.5, and 1.3 s for PT, TPT, and TECT, respectively. For fluid heat transfer analysis, two points were selected in the tubes, one at the tube center and the other at the tube outlet, to compare the heat transmission ability. Figure 8(a, c, e) demonstrates the fluid temperature at the selected points in the center. Figure 8(b, d, f) presents the exit fluid temperature. Temperatures at the center and outlet of PT, TPT, and TECT were monitored every millisecond until the end of the simulation. In Figure 8, the results of the predictions demonstrate that the variation of the fluid's temperature follows a similar pattern. As demonstrated in Figure 8(a), the temperature of the PT improves proportionally with time. There is a minor oscillation
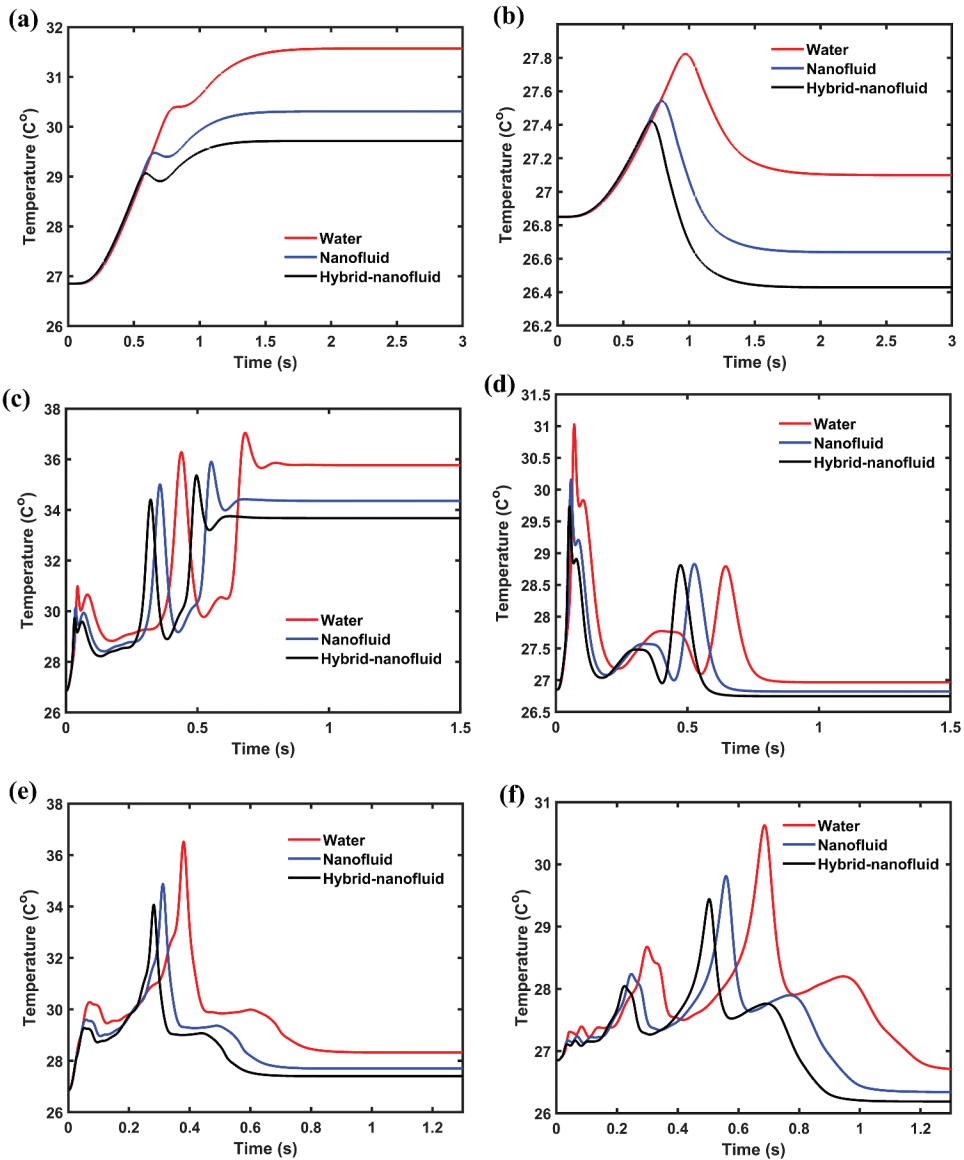
Figure 8. Curves of temperatures (a & b) for PT, (c & d) for TPT, and (e & f) for TECT.

at the beginning of the process as a consequence of excessive mesh refinement (Boz, Erdogdu, and Tutar 2014). This is in agreement with Boz, Erdogdu, and Tutar (2014) and Erdogdu and Tutar (2012). As seen in Figure 8(a), the highest temperature reached is 31.6Cº, 30.3Cº, and 29.7Cº for Al_2O_3-Cu /water, CuO/water, and water, respectively. The temperature differences are mostly determined by the fluid velocity (Wu et al. 2014). When hybrid nanofluid is applied as the working fluid in the plain pipe PT in Figure 8(b), the maximum temperature variation is reduced by around 4.1% and 6.2% when compared to water and nanofluid, respectively. Thus, employing a hybrid-nanofluid of Al_2O_3-Cu /water can increase heat transmission (Khfagi et al. 2022). This is owing to an increase in dynamic viscosity and thermal conductivity, as stated in Vajjha and Das (2008).

Figure 8(c–f) shows the temporal evolution of temperature for different fluids; TPT and TECT can be seen through (c and d) and (e and f), respectively. Based on Figure 8(c–f) the temperature difference
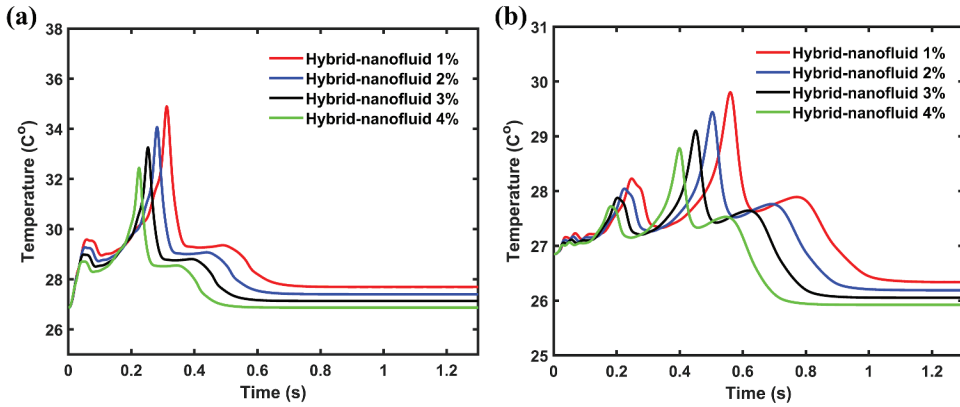
Figure 9. Temperature curves for TECT at different concentrations of Al_2O_3-Cu/water at (a) centre point (b) outlet fluid.

rose faster initially. This is because twisting tape makes the boundary layer less stable, which disrupts it and thus increases temperature distribution in the pipe. This is seen in Figures 4 and 5. These short-time fluctuations have been found in the literature, for example Heng et al. (2019) and Li et al. (2017). As a consequence of this breakup of the boundary layer, the heat transport rate is raised. This leads to a faster stabilization of the solution to the steady state. In pipes with solid and elliptical-cut twisted tapes, the temperature reaches steady-state after 0.8 s and 1 s, respectively. As displayed in Figure 8(c, e),
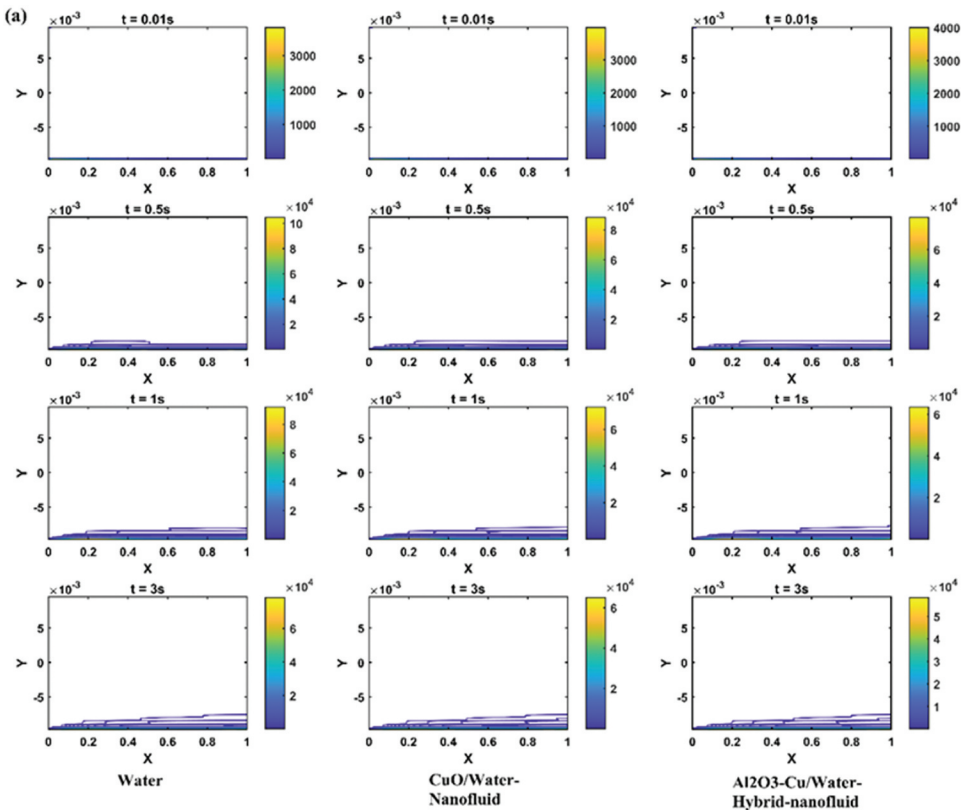

Figure 10. Spatio-temporal development of the rate of entropy formation owing to heat transmission in (a) (PT), (b) (TPT), and (c) (TECT) for different fluids at different times.
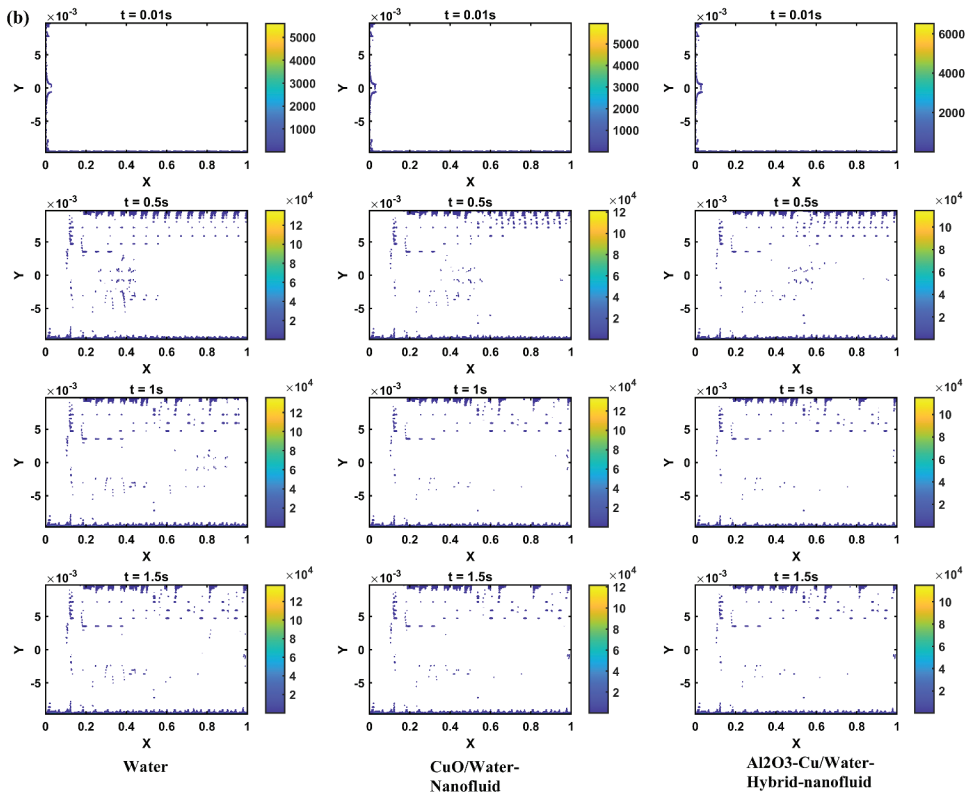
Figure 10. (continued).

the maximum temperature in the middle of the tube under water, CuO/water, and Al_2O_3-Cu/water changes by 10.8Cº, 9.4Cº, 8.7Cº for TPT, and 9.6Cº, 7.9Cº, 7Cº for TECT, respectively. The figure further shows that TPT and TECT have more uniformly high temperatures compared to PT. The reason for this is that the accelerated whirling of fluid within the tubes brought about by the twisted tape causes the layer of thermal barriers to break down, allowing for better flow mixing between the surface of the heating wall and the fluids at the center (Ahmadi et al. 2020; Oni and Paul 2016). Nonetheless, as displayed in Figure 8(s), the exit temperature of the water, nanofluid of CuO/water, and hybrid-nanofluid Al_2O_3-Cu/water decreased from about 31.1Cº, 30.1Cº, and 29.7Cº at $t = 0.1$ s to 27.9Cº, 26.8Cº, and 26.7Cº, to steady-stage (at $t = 1.5$ s), respectively. The lower exit temperatures of different fluids indicate the improvement of heat transfer (Zachar, Farkas, and Szlivka 2003). Depending on the time and tape geometries, the exit temperature of the flows in the pipe supplied with elliptical-cut twisted tape was improved as compared to those in the TPT by about 2%, 1.8%, and 1.1% for Al_2O_3-Cu/water, CuO/water, and water, respectively, as demonstrated in Figure 8(d, f). This could be partially attributed to the fact that there is heat transmission between the duct's wall and the plane of elliptical-cut and classical twisted tape, though the heat flow is non-uniform. Because of the rise in turbulence intensity, the thermal/velocity boundary layer is destroyed more efficiently (Ahmadi et al. 2020; Khfagi et al. 2022; Oni and Paul 2016). Solid and elliptical-cut twisted tape are applied to further enhance the heat transport during the transition time when hybrid-nanofluid is employed as the working fluid (Khfagi et al. 2022). For Al_2O_3-Cu/water at the center point, it is observed that the heat transport enhancement neared the quasi-steady state for a duration of approximately 1.4 s, 0.7 s, and 0.6 s and achieved higher values for a period of about 1.3 s, 0.4 s, and 0.3 s for PT, TPT, and TECT, respectively. Transient heat transfer increases exhibit a strong reliance on twisted tape geometries and applying Al_2O_3-Cu/water hybrid-nanofluid. This behavior is comparable to that of a plate heater (Liu, Shibahara, and Fukuda 2008).
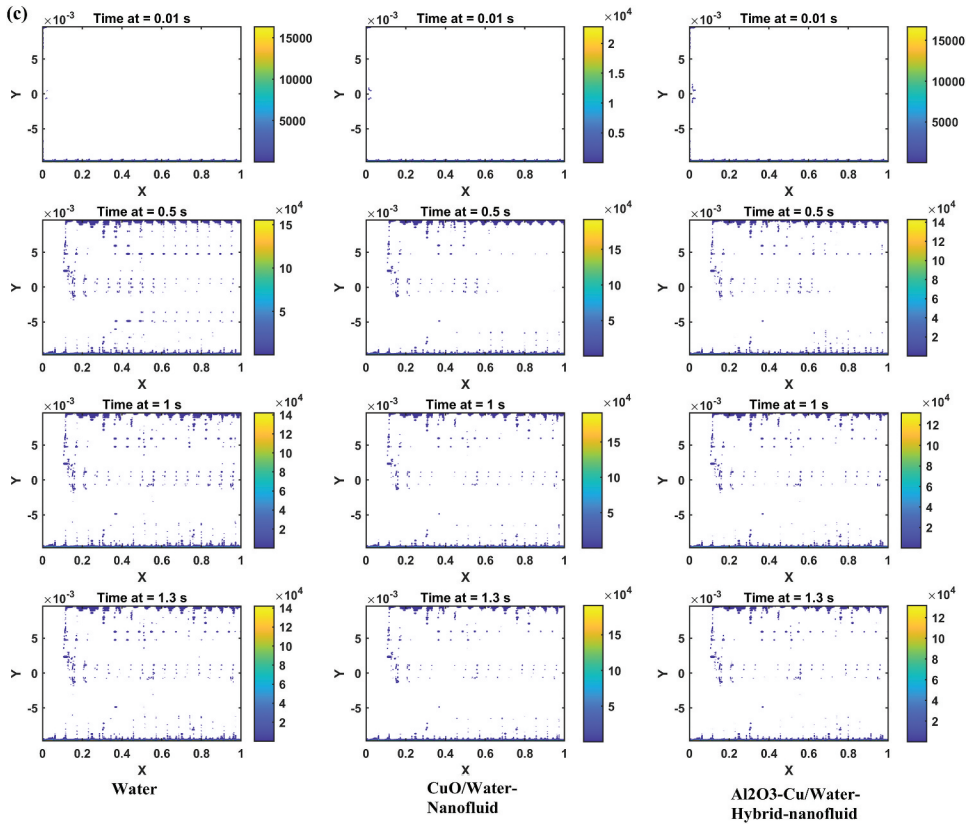
Figure 10. (continued).

Figure 9(a, b) displays the temperature curves for TECT at various concentrations of Al_2O_3-Cu/water at the selected points in the center and the exit fluid temperature, respectively. The predicted flow temperature of the fluid at different concentrations did not show any noticeable difference in the shape of the curve. Obviously, the temperature decreased as the concentration of nanoparticles increased. This means that the heat transmission is improved as the concentration of nanoparticles increases from 1% to 4%. Overall, when nanoparticles are added, the velocity and heat transmission rate were increased. Unsteady flows reach steady states as heat transfer and temperature gradient increase with increased time and flow rate.

Entropy generation analysis

This section presents a study analyzing entropy generation in transient heat transport for Al2O3-Cu/water, CuO/water, and plain water at $\varnothing = 2\%$ in PT, TPT, and TECT. Additionally, the total entropy production and Bejan number in TECT for Al_2O_3-Cu/water were assessed for $\varnothing$ ranging from 1% to 4%. Irreversible heat transmission and fluid friction are the sources of irreversibilities (entropy) (Zimparov 2001). Entropy production is a thermodynamic characteristic that provides insights into the distribution of parameters and the locations of prevalent irreversibility within the vortex tube. This search aims to calculate the contributions of heat transmission and fluid friction to entropy creation in a duct supplied with elliptical-cut and solid twisted tape during transient heat transfer.
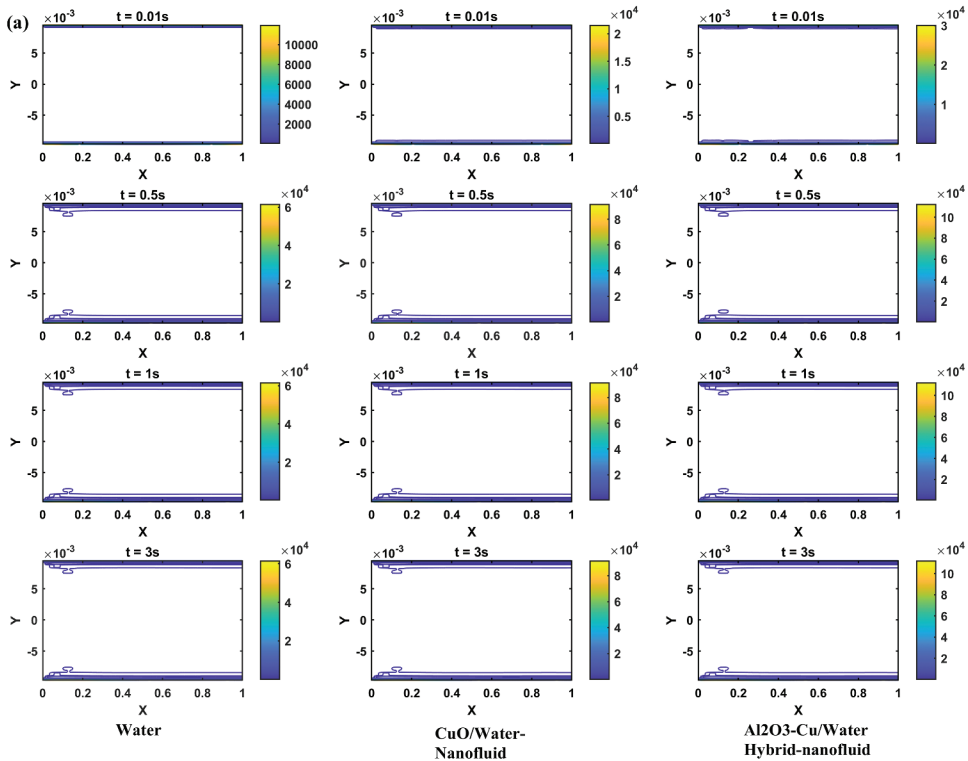
Figure 11. Spatio-temporal development of the rate of entropy creation owing to fluid friction in (a) (PT), (b) (TPT), and (c) (TECT) for different fluids at different times.

Local entropy production

The MATLAB code was used to examine the thermodynamic irreversibility of local entropy production during transient heat transport. Figures 10a and 11a illustrate local entropy production during transient heat transfer. For various time intervals, these figures plot the spatial distributions of entropy production by water, nanofluid, and hybrid-nanofluid. Heat transport is responsible for local entropy production for PT, TPT, and TECT, respectively. It is obvious from Figure 10 that at $t = 0.01$ s, thermal entropy is created by the endothermic process. However, heat transfer increases at $t = 0.5$ and 1 s. This trend matches previous research's numerical results (Khfagi et al. 2022). The final row in Figure 10(a–c) indicates that the operating time has ceased at 3 s, 1.5 s, and 1.3 s for PT, TPT, and TECT, respectively. Figure 10(a) reveals that in normal ducts, the area near the wall generates the highest thermal entropy, where there is a greater temperature difference. Figure 10(b, c) demonstrate that both solid and elliptical-cut twisting tape produce spatial distribution of thermal irreversibility, leading to intense eddy flow between the duct wall and the tape surface. This, in turn, increases thermal entropy. This behavior aligns with the observations made by Hunt et al. regarding heat transfer irreversibility (Hunt, Karimi, and Torabi 2018). However, it is evident from Figure 10(a–c) that the introduction of nanoparticles reduces thermal entropy production compared to a regular fluid, consistent with the findings of Refs (Esfahani et al. 2017; Khfagi et al. 2022). Notably, the advantage of hybrid nanofluids decreases the creation of thermal entropy. For instance, when applying hybrid-nanofluid in TECT (Figure 10(c)), the entropy production rate decreases by approximately 14.3% and 20% compared to water and nanofluid, respectively. Figure 11(a–c) proves the creation of local entropy due to fluid friction for PT, TPT, and TECT, respectively. The plots vary with time, displaying a symmetrical and transient flow pattern. Comparing these findings with the k-ε turbulence model results in Figure 7 reveals several similarities. Specifically, Figure 11(a), demonstrates that entropy formation is concentrated on the tube wall due to an orthogonal
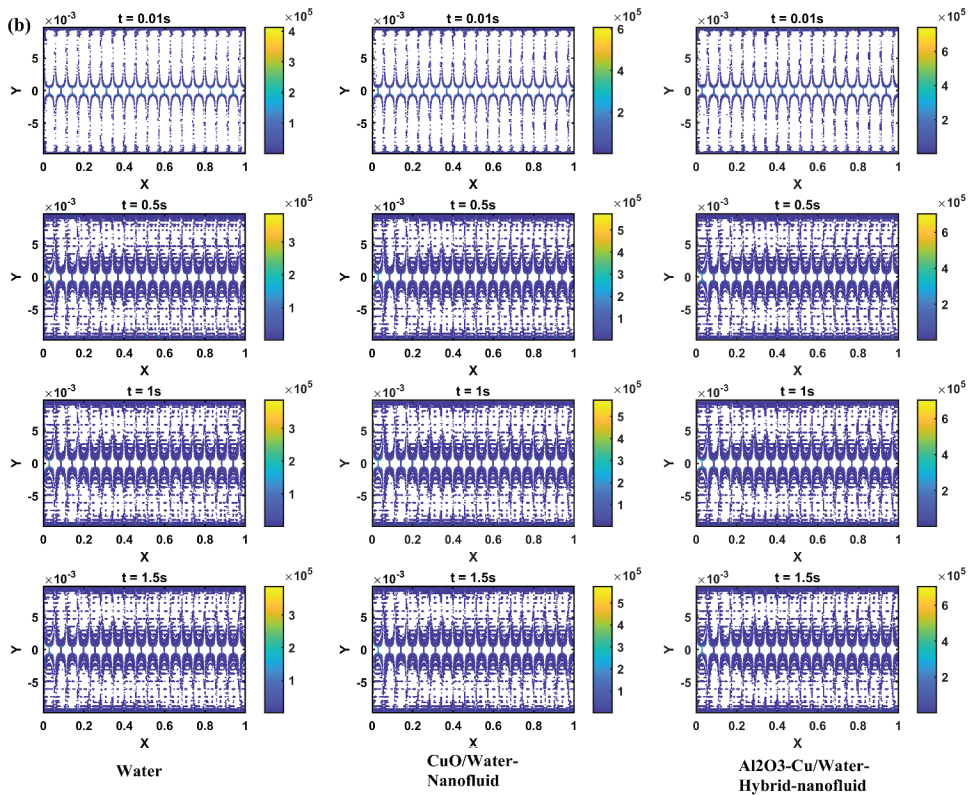
Figure 11. (continued).

velocity gradient. Frictional entropy production around the rotational axis of solid and elliptical-cut twisted tape significantly increases in the vicinity of the elliptical-cut and solid twisted tape regions in Figure 11(b, c). Additionally, the introduction of TPT and TECT enhances both heat transmission and entropy generation. This improvement is attributed to the elevated flow velocity gradients resulting from the benefit of twisted tape in this region. Figure 11c clearly shows that the inclusion of nanoparticles substantially contributes to the increase in frictional entropy production. The presence of nanoparticles enhances the fluid viscosity, thereby amplifying fluid friction (Malik and Nayak 2018). Notably, the TECT geometry has been found to reduce viscous entropy formation compared to TPT.

Entropy generation at current operating conditions
Figure 12 and 13 show the entropy generated due to fluid friction and heat transfer in the pipes (a) PT, (b) TPT, and (c) TECT with different fluids at $\varnothing = 2\%$. Figure 14(a, b) demonstrate the heat entropy and friction entropy production of TECT with Al_2O_3-Cu/water at concentrations from 1% to 4%, respectively. These figures provide important insights into transient entropy generation. The study found that the thermal entropy generated increased over time in all tubes tested. However, TECT produced lower thermal entropy than TPT and PT because it had improved heat transfer. This result is consistent with previous findings (Khfagi et al. 2022). Frictional entropy was increased by twisted tape and nanoparticles. However, thermal entropy production gradually decreased with increasing nano-particle concentrations, consistent with findings from previous research (Huminic and Huminic 2016). Al_2O_3-Cu/water at $\varnothing = 4\%$ was identified as a good working fluid due to its reduced entropy formation rate. These results are presented in Figures 12–14 of the study.
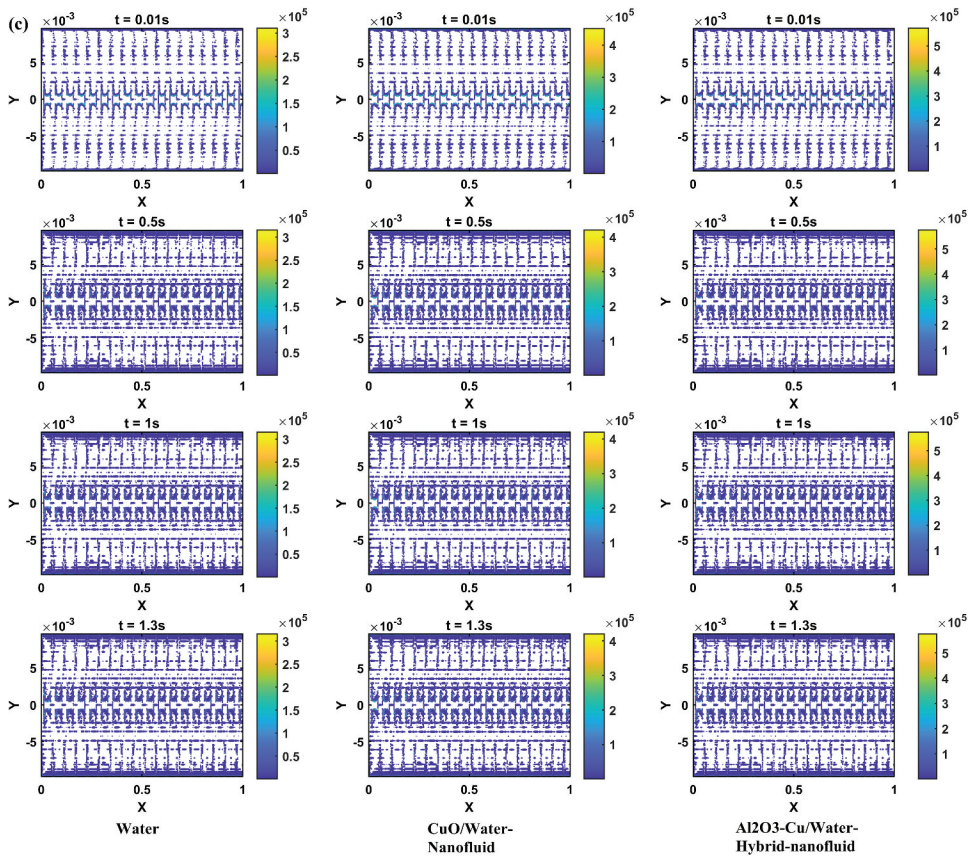
Figure 11. (continued).

Total entropy production

The total entropy production is influenced by the contributions of heat transmission and fluid friction. Figure 15(a–c) visually presents the cumulative creation of entropy across various fluid flows, including Al_2O_3-Cu/water hybrid-nanofluid, CuO/water nanofluid, and pure water, as well as three different designs denoted as PT, TPT, and TECT. The nanoparticle concentration is fixed at 2%, with four different time situations considered. In unstable conditions, entropy increases with time due to temperature penetration into the channel center, an increased temperature gradient, and the temperature gradient's dominance in the entropy equation. The results in Figure 15 indicate that the use of hybrid nanofluid and nanofluid leads to a decrease in total entropy production. The impact of TPT as well as TECT on the system's total irreversibility is evident in this figure. Total entropy generation slightly increases for both classical and elliptical-cut twisted tapes on very short-time scales. Swirling currents have a greater influence on temperature and velocity gradients, resulting in a slightly but variable increased total entropy generation rate. References (Belahmadi and Bessaih 2018; Esfahani et al. 2017) support the finding that increasing the nanoparticle volume fraction reduces total entropy production. The inclusion of plate and elliptical-cut twisted tape, as well as hybrid nanofluid, significantly affects the rate of decrease in total entropy production. For example, at $t = 1$ s, TPT and TECT exhibit a 50% and 54% reduction in total entropy production rates compared to PT, respectively. Furthermore, in TECT, the total entropy generation of Al_2O_3-Cu/water is reduced by 5.4% and 3% compared to water and CuO/water, respectively. Figure 16(a, b) presents the impact of hybrid nanofluid
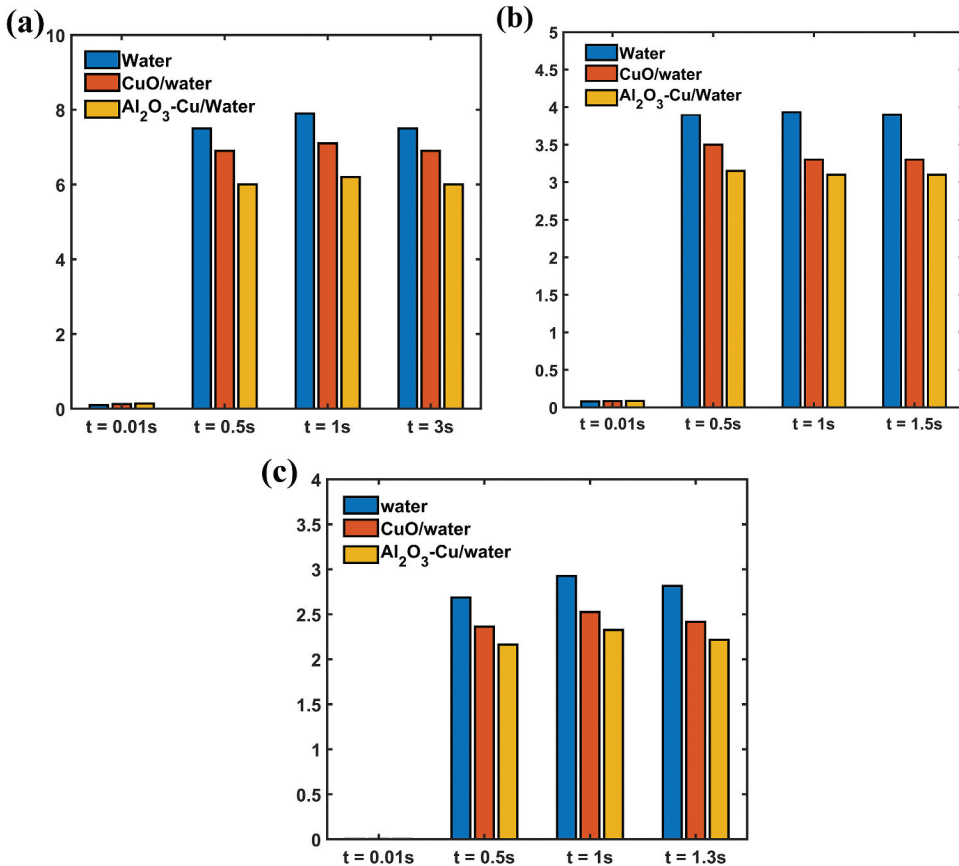
Figure 12. Entropy creation due to heat transmission in (a) (PT), (b) (TPT), and (c) (TECT) at different times.

concentration on total entropy production and the Bejan number for TECT. Increasing the nanoparticle concentration leads to an increase in the total entropy production rate due to higher frictional entropy production. Conversely, the Bejan number decreases with an increase in the number of nanoparticles, indicating a higher proportion of frictional entropy to total entropy and a decrease in the proportion of thermal entropy. This finding aligns with previous studies (Al-Rashed et al. 2019; Shahsavar, Moradi, and Bahiraei 2018). Hybrid nanofluid and tube geometry enhance transient heat transmission and reduce entropy creation. The simulation results of the proposed Al_2O_3-Cu/water and TECT are proven in Table 2. All data used in the comparisons are the best-observed findings from corresponding research. Novel Al_2O_3-Cu/water and TECT achieve better performance in the proposed work, where the temperature reached steady-state after 0.8s.

Conclusions

The impact of transient heat transmission enhancement and entropy production analysis in TECT, TPT, and PT under Al_2O_3-Cu/water hybrid turbulent nanofluid flow under non-uniform heat flux has been investigated numerically. Following is a summary of the results obtained:

- Heat flux obtained by numerical simulation was compared to numerical and experimental data to validate the results using Monte Carlo Ray-Trace (MCRT) approach.
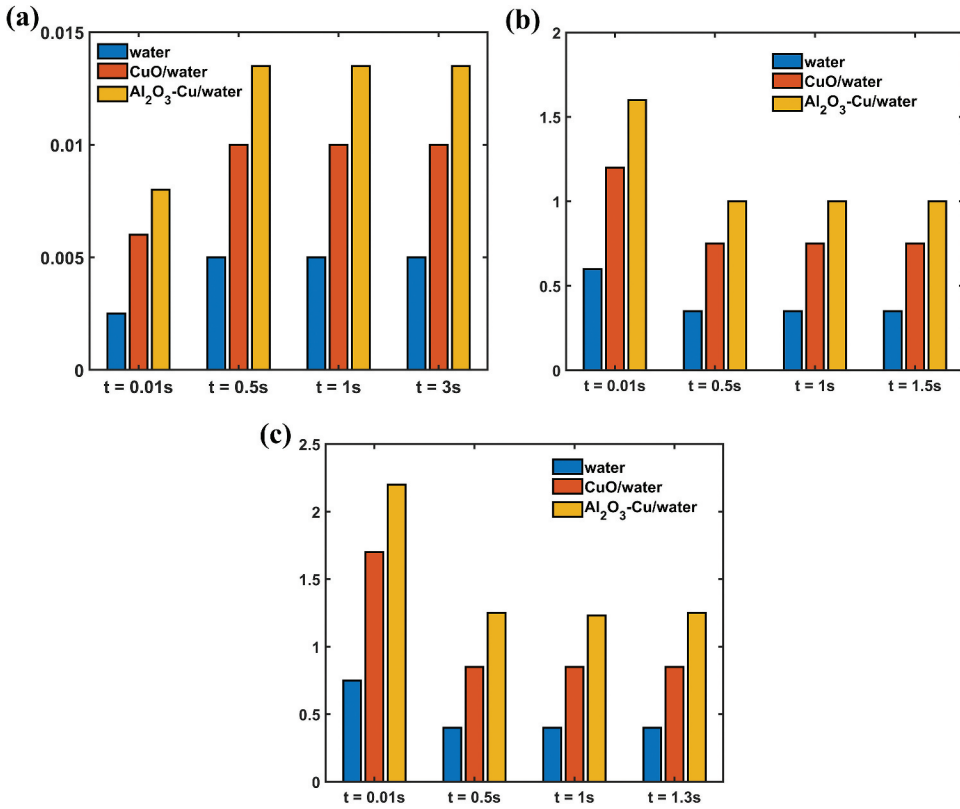
Figure 13. Entropy creation due to fluid friction in (a) (PT), (b) (TPT), and (c) (TECT) at different times.
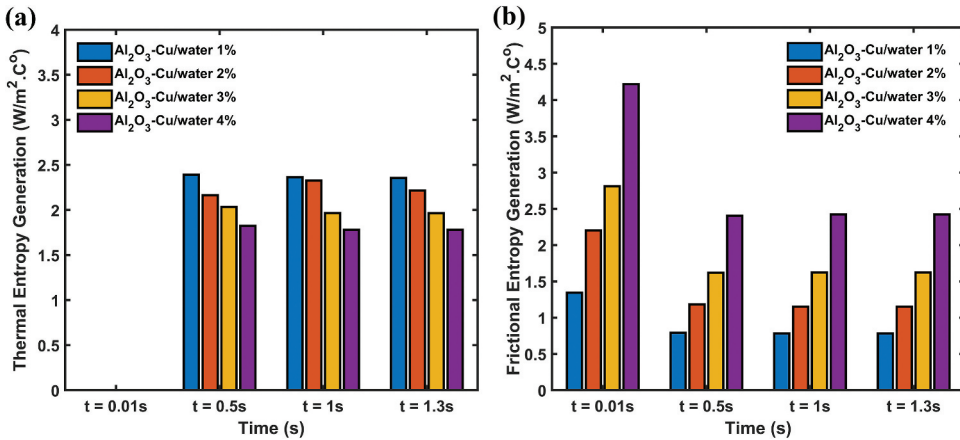
Figure 14. Entropy creation of Al_2O_3-Cu/water at different concentrations in TECT (a) thermal and (b) frictional.

- Through applying the hybrid nanofluid, the heat transfer rate is improved significantly. The impact of Al_2O_3-Cu/water hybrid nanofluid in this study shows a significant influence on heat transfer. The maximum temperature difference is reduced to around 4.1% and 6% when compared to water and nanofluid, respectively.
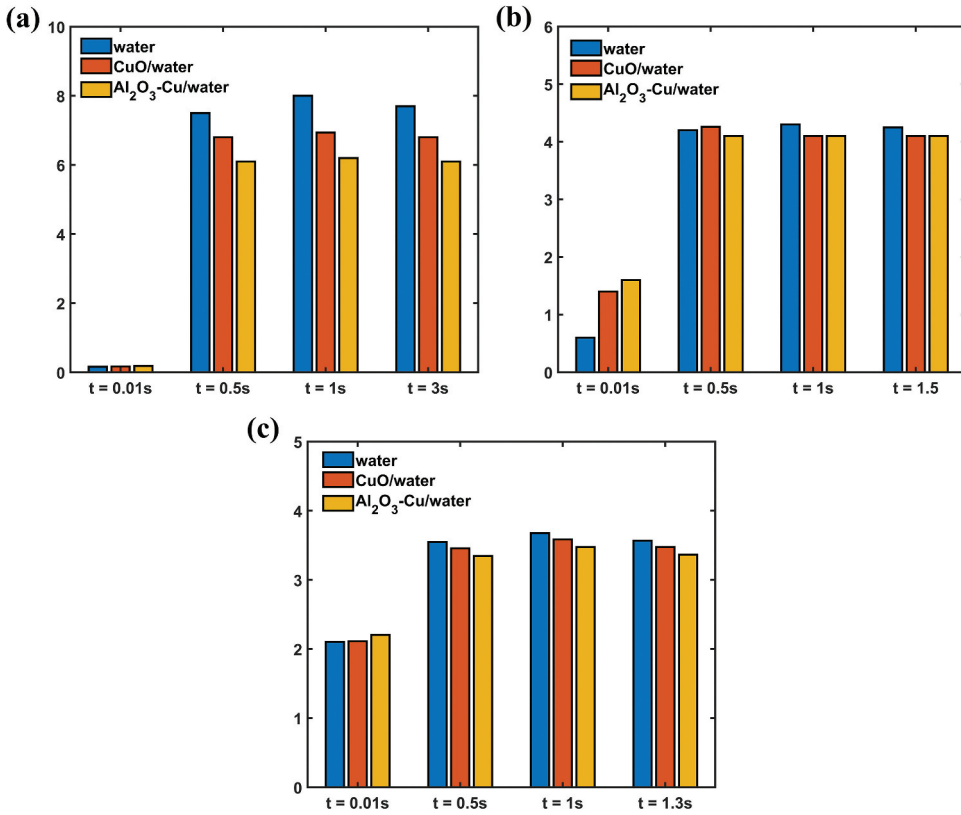
Figure 15. Total entropy production in (a) PT, (b) TPT, and (c) TECT at different times.
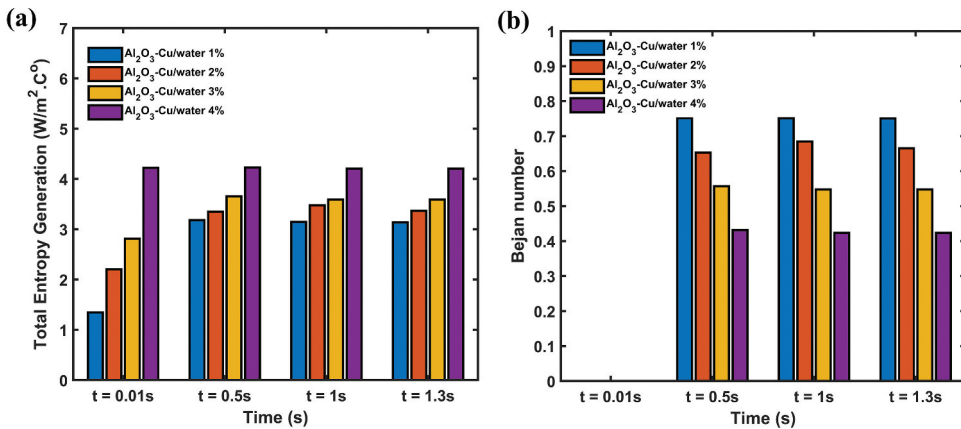
Figure 16. (a) creation of total entropy and (b) Bejan number for various concentrations of Al_2O_3-Cu/water in TECT.

- The elliptical-cut twisted tape (TECT) in this study shows a good augmentation in the heat transfer as compared to those in the TPT by about 1.1%, 1.8%, and 2% of water, CuO/water, and Al_2O_3-Cu/water, respectively.
- The addition of nanoparticles reduces thermal entropy creation by 20% and increases frictional entropy production.

Table 2. Summary of research findings.

References	Fluids	Transient heat transfer rate	Minimize total entropy generation
Proposed work	Al_2O_3-Cu/water	6.2%	54%
(Boz, Erdogdu, and Tutar 2014)	Water	5%	Null
(Li et al. 2019)	Water	5.53%	Null
(Wu et al. 2014)	water	6%	Null
(Malik and Nayak 2018)	Cu–water	Null	43.1%

- Total entropy production rates in TPT and TECT are decreased by 50% and 54%, respectively, when compared with PT.
- Irreversibility in this problem is dominated by frictional entropy production.
- Minimization of the total entropy production may be sought by applying hybrid-nanofluid and using TECT.

The unsteady flow of mixed convection in pipes fitted with twisted tape has not received adequate attention from a second-law analysis perspective.

Nomenclature

a	Diameter-cut width (m)
b	Diameter-cut long (m)
Be	Bejan number (-)
C_1, C_2, C_μ	Model constants (-)
C_p	Specific heat (J Kg^{-1} C^{-1})
D	Pipe diameter (m)
f	Friction Factor (-)
G_k	Production of turbulent kinetic energy (J Kg^{-1})
h	Heat transfer coefficient (W m^{-2} C^{-1})
k	Turbulent kinetic energy (J Kg^{-1})
k_c	Thermal conductivity (W m^{-1} C^{-1})
L	Length of duct (m)
Nu	Nusselt number (-)
P	Pressure (Pa)
Re	Reynolds number (-)
S_{ij}	Linear distortion rate (-)
$S_{F,F}$	Fractional entropy creation (W m^{-3} C^{-1})
t	Time (s)
T	Fluid temperature (C)
u	Velocity (m s^{-1})
w	Width of twisted tape (m)
y	Twisted tape pitch (m)
Greek Symbols	
ρ	Density (Kg m^{-3})
$\emptyset$	Solid volume fraction (-)
μ	Dynamic viscosity (Pa-S)
τ_w	Wall shear stress (Pa)
η	Thermal efficiency factor (-)
δ	Thickness (m)
σ_ε	Model constant (-)
Δp	Drop of pressure (Pa)
Acronyms	
PT	Plain pipe
TECT	Twisted pipe with elliptical cut
TPT	Classical twisted tape

Acknowledgements

Disclosure statement

Funding

Notes on contributors

Dr Amir Khfagi I completed my first degree in mechanical engineering in 2003 at Ajdabya faculty of engineering in Libya. This was followed by a master's degree in advanced mechanical engineering at Sheffield Hallam University 2015. I was accepted to the University of Glasgow to study for a PhD in Mechanical Engineering in June 2019. I completed my PhD in June 2023 in the investigation of entropy generation and thermohydraulics of forced and mixed convection of Al2O3-Cu/water in a parabolic trough receiver tube.

Dr Graeme Hunt I completed my first degree in Chemistry at the University of St Andrews in 1994. Following many years working outside of academia, I completed a further degree in Mathematics at the Open University. I was accepted to the University of Glasgow to study for a PhD in Mechanical Engineering in 2015 and won a scholarship to fund it. I completed my PhD on non-equilibrium thermodynamics in porous media in early 2020 and have worked as a PDRA on multiple projects at the University of Glasgow since then.

Prof. Manosh C Paul Professor of Thermofluids at Mechanical Engineering and member of the Energy and Sustainability Group within the Systems, Power & Energy Research Division of the James Watt School of Engineering, University of Glasgow, UK. Recently, he held a prestigious RAEng/Leverhulme Trust Senior Research Fellowship. He joined the University of Glasgow in August 2003 as a Lecturer, and was promoted to Senior Lecturer in 2013, Reader in 2017, and Professor in 2020. Prior to Glasgow, he was a PDRA at the Department of Mechanical Engineering of Imperial College London. He received his PhD in Thermofluids in 2002 from the Department of Mechanical Engineering, University of Bath. He has first class degrees, with distinctions and gold medals, in both MSc (Applied Mathematics) and BSc honours (Mathematics) obtained from the University of Dhaka in 1999 and 1997 respectively. He is a Chartered Engineer (CEng), Fellow of the Higher Education Academy (FHEA), and member of the Engineering Professors' Council, Institution of Mechanical Engineers (IMechE), UK Combustion Institute, and International Association of Engineers (IAENG).

Dr Nader Karimi completed his first degree in mechanical engineering in 2000 at AmirKabir University of Technology in Tehran/Iran. This was followed by a master's degree in energy conversion at Sharif University of Technology, Tehran in 2003. He was awarded a PhD in 2009 for his experimental and theoretical work on unsteady combusting flows at University of Melbourne in Australia. In between 2009 and 2011, he was a Marie Currie post-doctoral researcher at Darmstadt University of Technology in Germany. He then moved to the Department of Engineering at University of Cambridge in the UK and worked there as a research associate for almost two years. In late 2013, he was appointed as a lecturer in mechanical engineering at James Watt School of Engineering, University of Glasgow where he served till early 2020. Nader is currently a Reader in Mechanical Engineering at the School of Engineering and Materials Science, Queen Mary University of London.

ORCID

Nader Karimi 🔵 http://orcid.org/0000-0002-4559-6245

References

Abuhatira, A. A., S. M. Salim, and J. B. Vorstius (2021). *Numerical simulation of turbulent pipe flow with 90-degree elbow using wall y+ approach.* Paper presented at the ASME International Mechanical Engineering Congress and Exposition.

Afsharpanah, F., A. Z. Sheshpoli, K. Pakzad, and S. S. M. Ajarostaghi. 2021. Numerical investigation of non-uniform heat transfer enhancement in parabolic trough solar collectors using dual modified twisted-tape inserts. *Journal of Thermal Engineering* 7 (1):133–47. doi:10.18186/thermal.846584.

Ahmadi, K., S. Khanmohammadi, S. Khanmohammadi, M. Bahiraei, and Q.-V. Bach. 2020. Heat transfer assessment of turbulent nanofluid flow in a circular pipe fitted with elliptical-cut twisted tape inserts. *Journal of Thermal Analysis and Calorimetry* 147 (1):727–40. doi:10.1007/s10973-020-10338-1.

Al-Rashed, A. A., R. Ranjbarzadeh, S. Aghakhani, M. Soltanimehr, M. Afrand, and T. K. Nguyen. 2019. Entropy generation of boehmite alumina nanofluid flow through a minichannel heat exchanger considering nanoparticle shape effect. *Physica A: Statistical Mechanics and Its Applications* 521:724–36. doi:10.1016/j.physa.2019.01.106.

Anderson, J. D., and J. Wendt. 1995. *Computational fluid dynamics*, Vol. 206. US: Springer.

Bejan, A. 2013. *Entropy generation minimization: The method of thermodynamic optimization of finite-size systems and finite-time processes*. CRC press.

Belahmadi, E., and R. Bessaïh. 2018. Heat transfer and entropy generation analysis of Cu-water nanofluid in a vertical channel. *World Journal of Engineering* 15 (5):604–13. doi:10.1108/wje-11-2017-0376.

Boz, Z., F. Erdogdu, and M. Tutar. 2014. Effects of mesh refinement, time step size and numerical scheme on the computational modeling of temperature evolution during natural-convection heating. *Journal of Food Engineering* 123:8–16. doi:10.1016/j.jfoodeng.2013.09.008.

Burkholder, F., and C. Kutscher. 2008. *Heat-loss testing of solel's UVAC3 parabolic trough receiver*. Golden, CO (United States): National Renewable Energy Lab.

Chang, C., X. Li, and Q. Zhang. 2014. Experimental and numerical study of the heat transfer characteristics in solar thermal absorber tubes with circumferentially non-uniform heat flux. *Energy Procedia* 49:305–13. doi:10.1016/j.egypro.2014.03.033.

Chang, C., C. Xu, Z. Wu, X. Li, Q. Zhang, and Z. Wang. 2015. Heat transfer enhancement and performance of solar thermal absorber tubes with circumferentially non-uniform heat flux. *Energy Procedia* 69:320–27. doi:10.1016/j.egypro.2015.03.036.

Dixon, A. G., M. Nijemeisland, and E. H. Stitt. 2006. Packed tubular reactor modeling and catalyst design using computational fluid dynamics. *Advances in Chemical Engineering* 31:307–89.

Erdogdu, F., and M. Tutar. 2012. A computational study for axial rotation effects on heat transfer in rotating cans containing liquid water, semi-fluid food system and headspace. *International Journal of Heat and Mass Transfer* 55 (13–14):3774–88. doi:10.1016/j.ijheatmasstransfer.2012.03.031.

Esfahani, J., M. Akbarzadeh, S. Rashidi, M. Rosen, and R. Ellahi. 2017. Influences of wavy wall and nanoparticles on entropy generation over heat exchanger plat. *International Journal of Heat and Mass Transfer* 109:1162–71. doi:10.1016/j.ijheatmasstransfer.2017.03.006.

Esmaeilzadeh, E., H. Almohammadi, A. Nokhosteen, A. Motezaker, and A. Omrani. 2014. Study on heat transfer and friction factor characteristics of γ-Al2O3/water through circular tube with twisted tape inserts with different thicknesses. *International Journal of Thermal Sciences* 82:72–83. doi:10.1016/j.ijthermalsci.2014.03.005.

Heng, S. Y., Y. Asako, T. Suwa, and K. Nagasaka. 2019. Transient thermal prediction methodology for parabolic trough solar collector tube using artificial neural network. *Renewable Energy* 131:168–79. doi:10.1016/j.renene.2018.07.037.

Hepbasli, A., and Z. Alsuhaibani. 2011. A key review on present status and future directions of solar energy studies and applications in Saudi Arabia. *Renewable and Sustainable Energy Reviews* 15 (9):5021–50. doi:10.1016/j.rser.2011.07.052.

He, Y.-L., J. Xiao, Z.-D. Cheng, and Y.-B. Tao. 2011. A MCRT and FVM coupled simulation method for energy conversion process in parabolic trough solar collector. *Renewable Energy* 36 (3):976–85. doi:10.1016/j.renene.2010.07.017.

Huminic, G., and A. Huminic. 2016. Heat transfer and entropy generation analyses of nanofluids in helically coiled tube-in-tube heat exchangers. *International Communications in Heat and Mass Transfer* 71:118–25. doi:10.1016/j.icheatmasstransfer.2015.12.031.

Hunt, G., N. Karimi, and M. Torabi. 2018. Two-dimensional analytical investigation of coupled heat and mass transfer and entropy generation in a porous, catalytic microreactor. *International Journal of Heat and Mass Transfer* 119:372–91. doi:10.1016/j.ijheatmasstransfer.2017.11.118.

Jafaryar, M., M. Sheikholeslami, and Z. Li. 2018. CuO-water nanofluid flow and heat transfer in a heat exchanger tube with twisted tape turbulator. *Powder Technology* 336:131–43. doi:10.1016/j.powtec.2018.05.057.

Jaramillo, O., M. Borunda, K. Velazquez-Lucho, and M. Robles. 2016. Parabolic trough solar collector for low enthalpy processes: an analysis of the efficiency enhancement by using twisted tape inserts. *Renewable Energy* 93:125–41. doi:10.1016/j.renene.2016.02.046.

Jeter, S. M. 1987. Analytical determination of the optical performance of practical parabolic trough collectors from design data. *Solar Energy* 39 (1):11–21. doi:10.1016/S0038-092X(87)80047-6.

Khfagi, A. M., G. Hunt, M. C. Paul, and N. Karimi. 2022. Computational analysis of heat transfer augmentation and thermodynamic irreversibility of hybrid nanofluids in a tube fitted with classical and elliptical-cut twisted tape inserts. *Journal of Thermal Analysis and Calorimetry* 147 (21):1–18. doi:10.1007/s10973-022-11418-0.

Khfagi, A. M., G. Hunt, M. C. Paul, and N. Karimi. 2023. Entropy generation and thermohydraulics of mixed convection of hybrid-nanofluid in a vertical tube fitted with elliptical-cut twisted tape inserts-a computational study. *Energy Sources, Part A: Recovery, Utilization, & Environmental Effects* 45 (2):3369–91. doi:10.1080/15567036.2023.2194855.

Kinoshita, H., T. Yoshida, H. Nariai, and F. Inasaka. 1996. Study on the mechanism of critical heat flux enhancement for subcooled flow boiling in a tube with internal twisted tape under nonuniform heating conditions. *Heat Transfer-Japanese Research: Co-Sponsored by the Society of Chemical Engineers of Japan and the Heat Transfer Division of ASME* 25 (5):293–307. doi:10.1002/(SICI)1520-6556(1996)25:5<293:AID-HTJ3>3.0.CO;2-S.

Krüger, D., Y. Pandian, K. Hennecke, and M. Schmitz. 2008. Parabolic trough collector testing in the frame of the REACt project. *Desalination* 220 (1–3):612–18. doi:10.1016/j.desal.2007.04.062.

Langtry, R. B. 2006. A correlation-based transition model using local variables for unstructured parallelized CFD codes. Ph.D thesis., University of Stuttgart.

Li, W., M. Paul, H. Baig, J. Siviter, A. Montecucco, T. Mallick, and A. Knox. 2019. A three-point-based electrical model and its application in a photovoltaic thermal hybrid roof-top system with crossed compound parabolic concentrator. *Renewable Energy* 130:400–15. doi:10.1016/j.renene.2018.06.021.

Li, W., M. Paul, M. Rolley, T. Sweet, M. Gao, H. Baig, and E. F. Fernandez, T. K. Mallick, A. Montecucco, J. Siviter. 2017. A coupled optical-thermal-electrical model to predict the performance of hybrid PV/T-CCPC roof-top systems. *Renewable Energy* 112:166–86. doi:10.1016/j.renene.2017.05.012.

Liu, Q., M. Shibahara, and K. Fukuda. 2008. Transient heat transfer for forced convection flow of helium gas over a horizontal plate. *Experimental Heat Transfer* 21 (3):206–19. doi:10.1080/08916150802072859.

Liu, Q., Z. Zhao, and K. Fukuda. 2014. Transient heat transfer for forced flow of helium gas along a horizontal plate with different widths. *International Journal of Heat and Mass Transfer* 75:433–41. doi:10.1016/j.ijheatmasstransfer.2014.03.077.

Liu, Q., Z. Zhao, and K. Fukuda. 2015. Experimental study on transient heat transfer enhancement from a twisted plate in convection flow of helium gas. *International Journal of Heat and Mass Transfer* 90:1160–69. doi:10.1016/j.ijheatmasstransfer.2015.07.061.

Malik, S., and A. Nayak. 2018. Effect of moving walls on heat transfer and entropy generation in a nanofluid-filled enclosure. *Journal of Engineering Mathematics* 110 (1):147–65. doi:10.1007/s10665-017-9941-7.

Marugán-Cruz, C., O. Flores, D. Santana, and M. García-Villalba. 2016. Heat transfer and thermal stresses in a circular tube with a non-uniform heat flux. *International Journal of Heat and Mass Transfer* 96:256–66. doi:10.1016/j.ijheatmasstransfer.2016.01.035.

Muñoz, J., and A. Abánades. 2011. Analysis of internal helically finned tubes for parabolic trough design by CFD tools. *Applied Energy* 88 (11):4139–49. doi:10.1016/j.apenergy.2011.04.026.

Mwesigye, A., T. Bello-Ochende, and J. P. Meyer. 2013. Numerical investigation of entropy generation in a parabolic trough receiver at different concentration ratios. *Energy* 53:114–27. doi:10.1016/j.energy.2013.03.006.

Mwesigye, A., T. Bello-Ochende, and J. P. Meyer. 2014. Minimum entropy generation due to heat transfer and fluid friction in a parabolic trough receiver with non-uniform heat flux at different rim angles and concentration ratios. *Energy* 73:606–17. doi:10.1016/j.energy.2014.06.063.

Mwesigye, A., T. Bello-Ochende, and J. P. Meyer. 2016. Heat transfer and entropy generation in a parabolic trough receiver with wall-detached twisted tape inserts. *International Journal of Thermal Sciences* 99:238–57. doi:10.1016/j.ijthermalsci.2015.08.015.

Nakhchi, M. E., and J. A. Esfahani. 2018. Cu-water nanofluid flow and heat transfer in a heat exchanger tube equipped with cross-cut twisted tape. *Powder Technology* 339:985–94. doi:10.1016/j.powtec.2018.08.087.

Oni, T. O., and M. C. Paul. 2016. Numerical investigation of heat transfer and fluid flow of water through a circular tube induced with divers' tape inserts. *Applied Thermal Engineering* 98:157–68. doi:10.1016/j.applthermaleng.2015.12.039.

Patankar, S. V., and D. B. Spalding. 1983. A calculation procedure for heat, mass and momentum transfer in three-dimensional parabolic flows. In *Numerical prediction of flow, heat transfer, turbulence and combustion*, 54–73. Elsevier.

Shahsavar, A., M. Moradi, and M. Bahiraei. 2018. Heat transfer and entropy generation optimization for flow of a non-Newtonian hybrid nanofluid containing coated CNT/Fe3O4 nanoparticles in a concentric annulus. *Journal of the Taiwan Institute of Chemical Engineers* 84:28–40. doi:10.1016/j.jtice.2017.12.029.

Sharma, K., L. S. Sundar, and P. Sarma. 2009. Estimation of heat transfer coefficient and friction factor in the transition flow with low volume concentration of Al2O3 nanofluid flowing in a circular tube and with twisted tape insert. *International Communications in Heat and Mass Transfer* 36 (5):503–07. doi:10.1016/j.icheatmasstransfer.2009.02.011.

Sheikholeslami, M., M. Jafaryar, and Z. Li. 2018. Second law analysis for nanofluid turbulent flow inside a circular duct in presence of twisted tape turbulators. *Journal of Molecular Liquids* 263:489–500. doi:10.1016/j.molliq.2018.04.147.

Shih, T.-H. 1993. *A realizable Reynolds stress algebraic equation model*, Vol. 105993. Kyoto, Japan: Lewis Research Center, Institute for Computational Mechanics in Propulsion.

Sundar, L. S., and K. Sharma. 2010. Turbulent heat transfer and friction factor of Al2O3 nanofluid in circular tube with twisted tape inserts. *International Journal of Heat and Mass Transfer* 53 (7–8):1409–16. doi:10.1016/j.ijheatmasstransfer.2009.12.016.

Tandiroglu, A. 2005. Second law analysis of transient heat transfer for turbulent flow in a circular tube with baffle inserts. *International Journal of Exergy* 2 (3):299–317. doi:10.1504/IJEX.2005.007257.

Tochio, D., and S. Nakagawa. 2011. Numerical simulation of three-dimensional thermal-hydraulic behavior for HTTR (high temperature Engineering test reactor). *Nuclear Engineering and Design* 241 (5):1616–26. doi:10.1016/j.nucengdes.2011.01.032.

Vajjha, R. S., and D. K. Das (2008). *Measurements of specific heat and density of Al 2 O 3 nanofluid*. Paper presented at the AIP Conference Proceedings, USA.

Versteeg, H. K., and W. Malalasekera. 2007. *An introduction to computational fluid dynamics: The finite volume method*. UK: Pearson education.

Wu, Z., S. Li, G. Yuan, D. Lei, and Z. Wang. 2014. Three-dimensional numerical study of heat transfer characteristics of parabolic trough receiver. *Applied Energy* 113:902–11. doi:10.1016/j.apenergy.2013.07.050.

Xu, L., Z. Wang, X. Li, G. Yuan, F. Sun, and D. Lei. 2013. Dynamic test model for the transient thermal performance of parabolic trough solar collectors. *Solar Energy* 95:65–78. doi:10.1016/j.solener.2013.05.017.

Yang, X., X. Yang, J. Ding, Y. Shao, and H. Fan. 2012. Numerical simulation study on the heat transfer characteristics of the tube receiver of the solar thermal power tower. *Applied Energy* 90 (1):142–47. doi:10.1016/j.apenergy.2011.07.006.

Zachar, A., I. Farkas, and F. Szlivka. 2003. Numerical analyses of the impact of plates for thermal stratification inside a storage tank with upper and lower inlet flows. *Solar Energy* 74 (4):287–302. doi:10.1016/S0038-092X(03)00188-9.

Zimparov, V. 2001. Extended performance evaluation criteria for enhanced heat transfer surfaces: heat transfer through ducts with constant heat flux. *International Journal of Heat and Mass Transfer* 44 (1):169–80. doi:10.1016/s0017-9310(00)00074-0.